Electronic Supplementary Material (ESI) for Nanoscale.
This journal is © The Royal Society of Chemistry 2017

Supporting Information for

High surface coverage of a self-assembled monolayer by *in situ* synthesis of palladium nanodeposits

Lucía Herrer, Víctor Sebastián, Santiago Martín, Alejandro González-Orive, Francesc Pérez-Murano, Paul J. Low, José Luis Serrano, Jesús Santamaría, and Pilar Cea

1. AFM characterization of a monolayer of 1 onto Au(111).

The average thickness of the **1** SAM was obtained by scratching the organic layer with the AFM tip in a 500 x 125 nm^2 area, Figure S1. Then, by subtracting the height of the bare gold substrate (unveiled after removing the organic film) from that of the surrounding molecule layer, the thickness of the film was obtained. Accordingly, a representative cross section together with a detailed statistical analysis of the depth distributions corresponding to the organic layer and the bare Au(111) terrace surfaces are depicted in Figure S1c and Figure S1d, respectively. Both contributions are fitted separately to Gaussian functions whose maximum difference allows an accurate estimation of the layer thickness, i.e. 1.78 ± 0.14 nm.

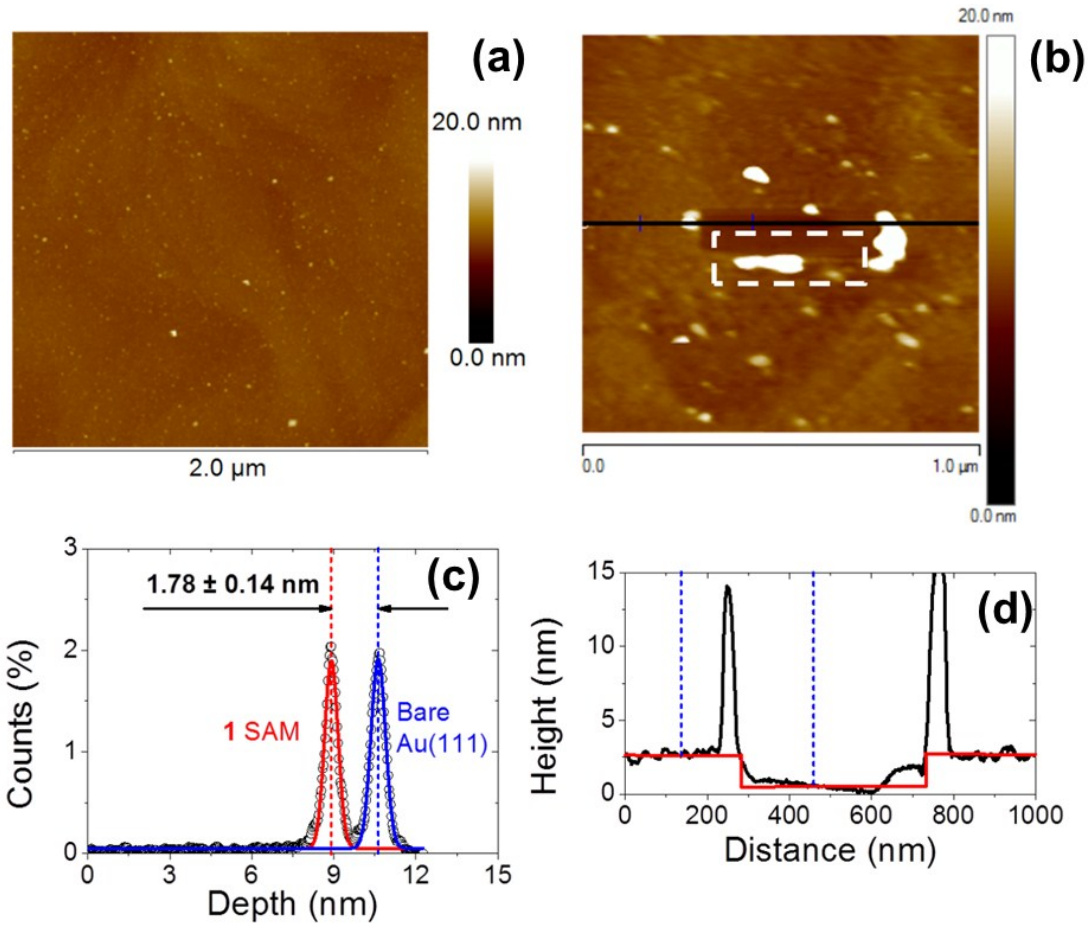

Figure S1. (a) 2.0 x 2.0 μm^2 AFM image showing the topography of an **1** monolayer-modified Au(111) surface. (b) 1.0 x 1.0 μm^2 AFM image of a 500 x 125 nm^2 scratch

made in a smooth Au(111) terrace covered by the organic layer, (c) depth profile histogram corresponding to the dashed white-boxed 400 x 100 nm^2 area, exhibiting the depth value distributions related to bare gold, blue line, and **1** layer, red. From the height difference between the later, the thickness of the **1** layer, i.e. 1.8 nm, can be obtained; (d) representative cross-section profile across the scratch.

2. XPS spectra

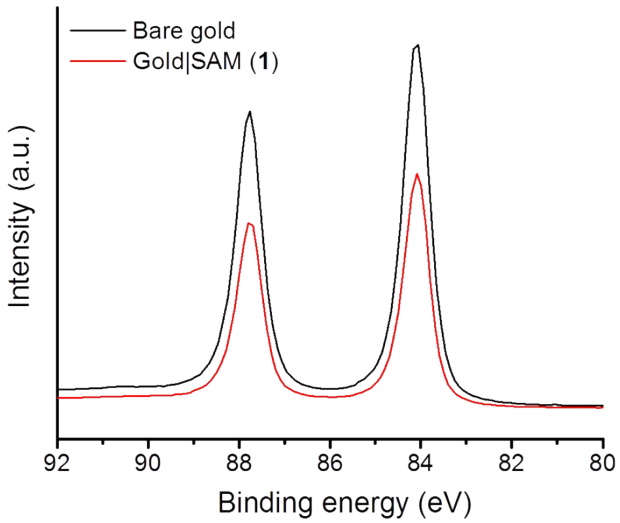

FigureS2. XPS spectra in the Au4f region for a bare gold electrode and a SAM of **1** deposited on gold.

3. CV of a monolayer of 1 onto Au(111).

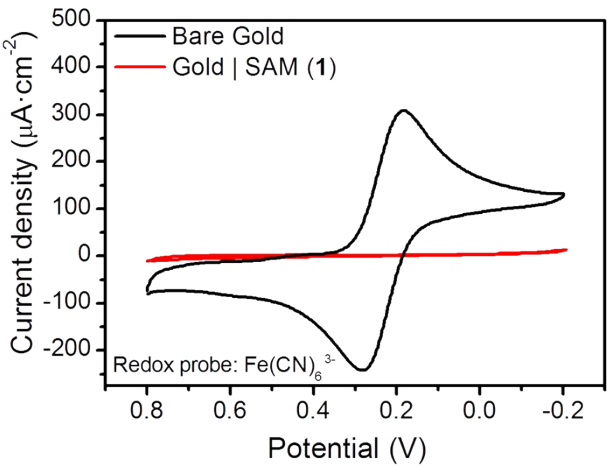

Figure S3. Cyclic voltammograms of a SAM of **1** deposited onto a gold electrode and comparison with the electrochemical response of a bare gold electrode. A bias voltage was applied to the working electrode immersed in aqueous solutions with 1 mM $K_3[Fe(CN)_6]$ and 0.1 M in KCl. The scan rate was 0.05 $V \cdot s^{-1}$ at 20 ºC and the initial scan direction was negative. The reference electrode was Ag/AgCl, KCl (3M).

4. Pd nanosheets from the bulk solution.

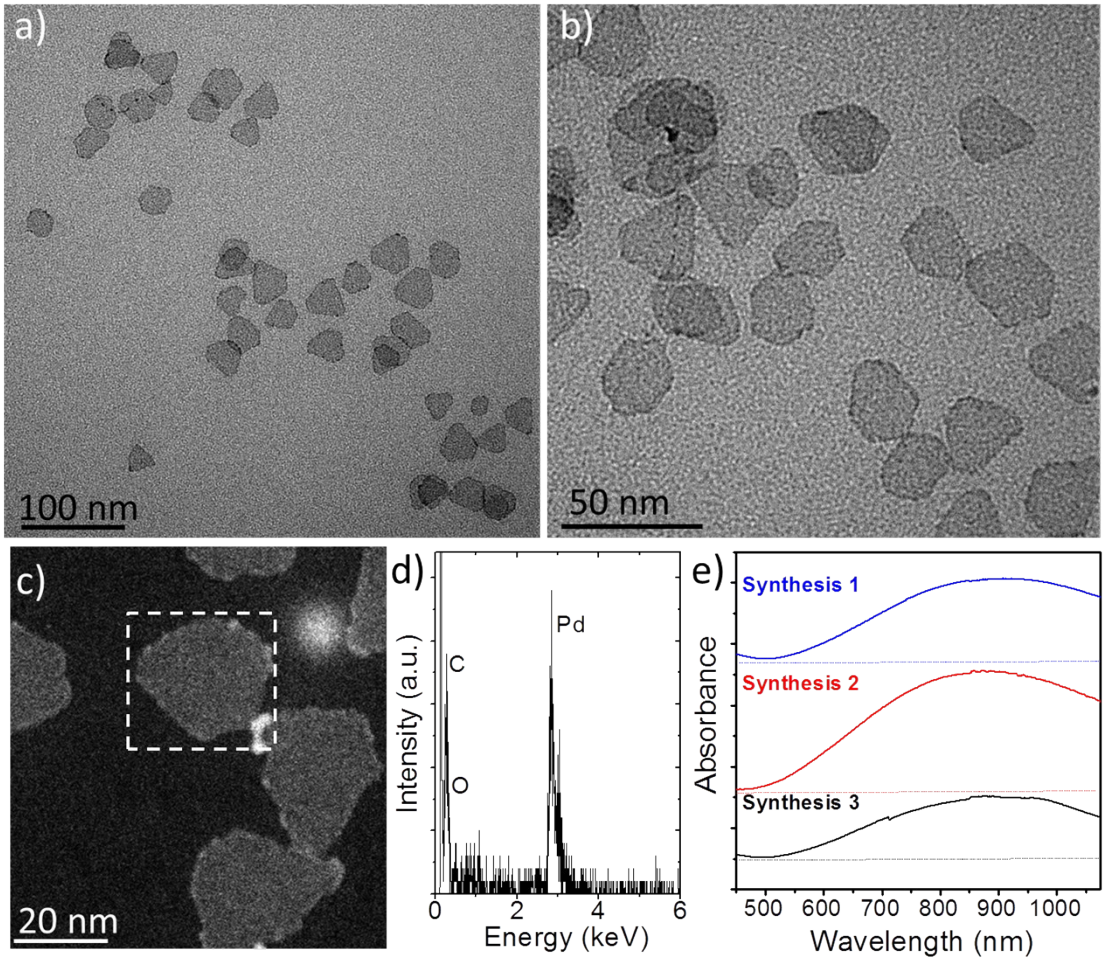

Figure S4. Pd nanosheets obtained in the resulting colloid. a-b) TEM images of Pd nanosheets with different magnification to support the selective growth of Pd to sheet like morphology; c) STEM-HAADF image of Pd nanosheets; d) EDS analysis of the area marked in c); e) UV-VIS spectra of several colloid samples resulted after synthesis.

5. **RMS roughness.**

Root Mean Squared (RMS) values were obtained for the monolayer film of **1** onto the Au(111) electrode, Figure S5a, and the PdNDs-modified monolayer of **1** deposited onto the Au(111) electrode, Figure S5b. In each case the RMS measurements were conducted on 300 x 300 nm^2 areas of the AFM images corresponding to one-single smooth terrace of the underlying Au(111) surface (to discard the influence of gold steps and grain boundaries), averaged over at least 30 AFM images extracted from different zones in each sample and also from distinct but equivalent samples.

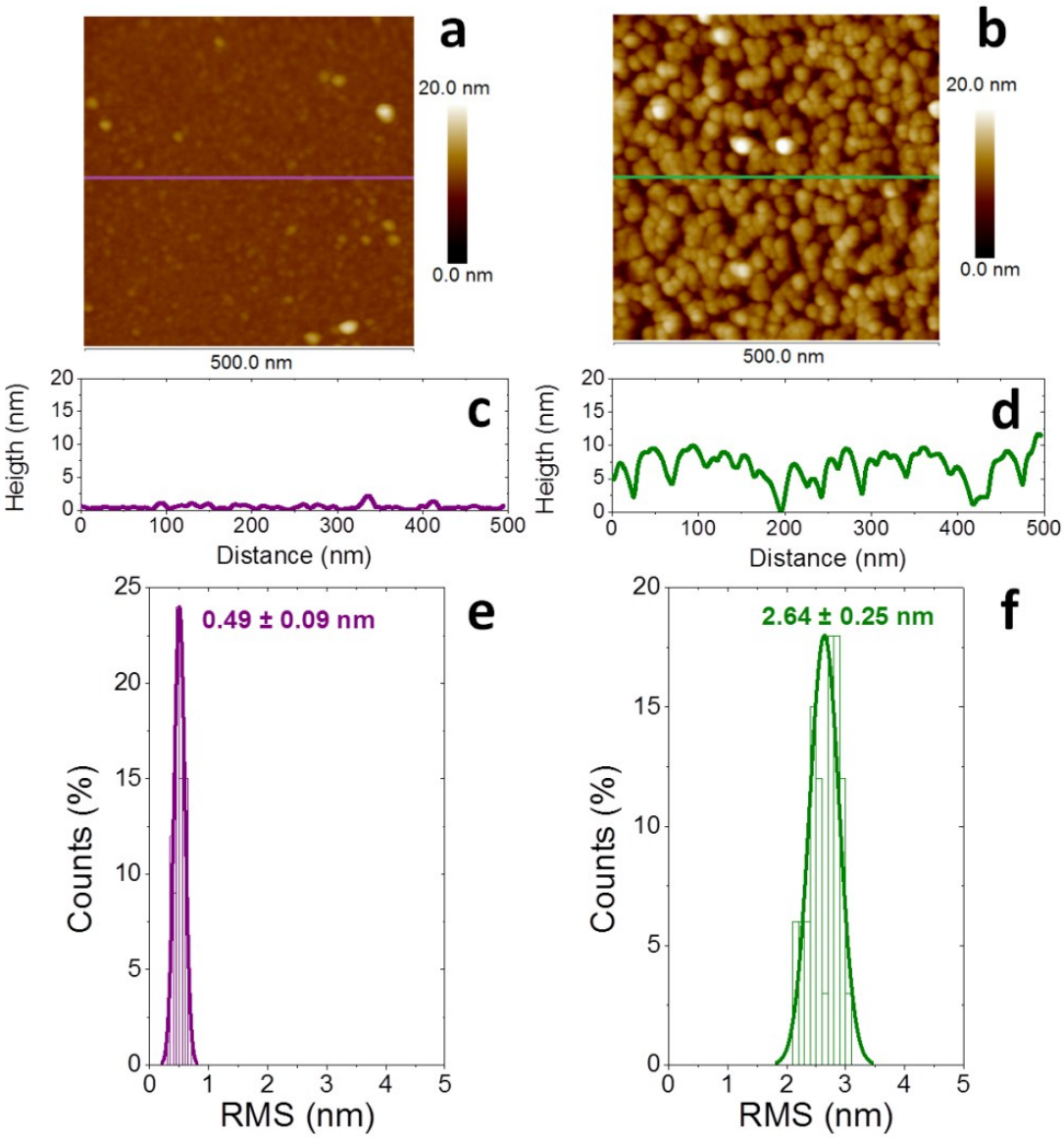

Figure S5. (a) 500 x 500 nm^2 AFM images showing the topography of a gold|SAM (**1**) and (b) gold|SAM (**1**)|PdNDs. (c) Representative cross-section profile across the lines drawn for gold|SAM (**1**) in purple line, and (d) gold|SAM (**1**)|PdNDs in green exhibiting their corresponding height value distributions. (e) Histogram showing the average RMS obtained for the gold|SAM (**1**) in purple line, and (f) histogram showing the average RMS obtained for the and gold|SAM (**1**)|PdNDs in green.

6. Size and height of PdNPs

Dimensions of PdNDs have been obtained by carrying out height profiles across AFM images, over more than 100 individual particles (Figure S5a and S5b). The statistical analysis of the data extracted from AFM images allows us to conclude that these PdNDs exhibit an average diameter of around 16 nm (corrected by the tip convolution) and an average height of ca. 7 nm. Histograms showing the height and diameter value distributions are depicted in Figures S6c and S6d, respectively.

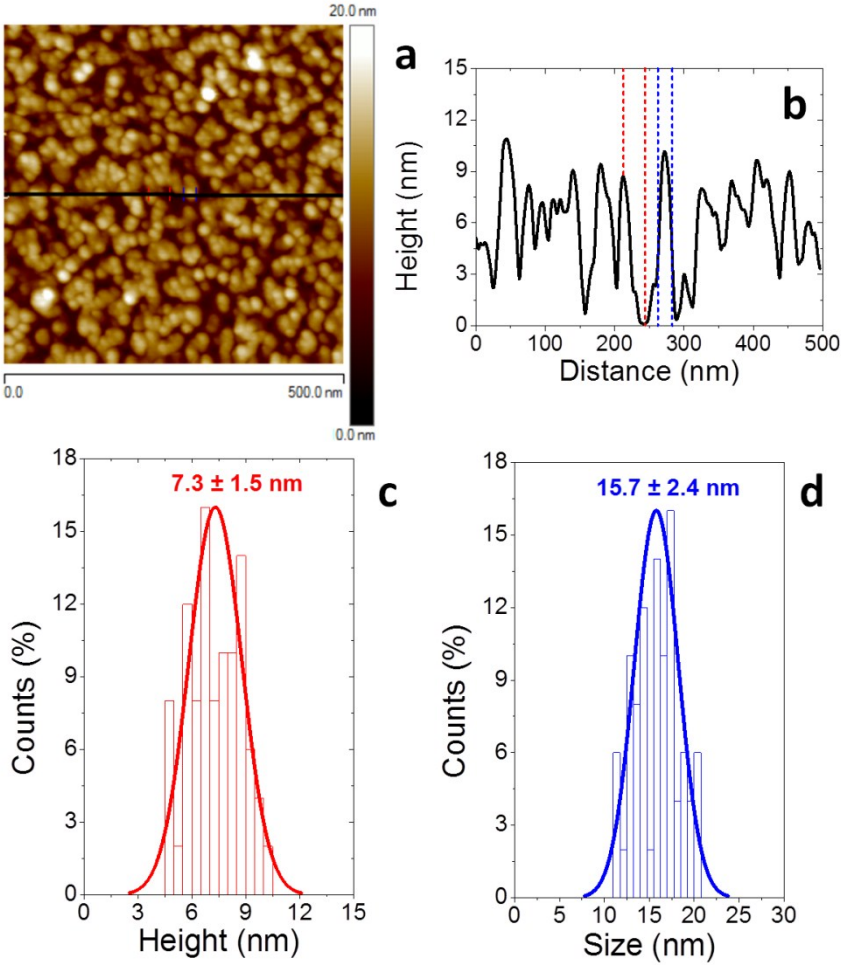

Figure S6. (a) 500 x 500 nm^2 AFM image of a monolayer film of **1** covered by PdNDs. (b) Representative cross section and analysis profile illustrating the dimensions of the measured PdNDs. (c) Histograms showing the particle diameter (blue line) and height distributions (red line) corresponding to 100 PdNDs proceeding from different AFM images. Averaged NDs diameter and height values are depicted in their respective graphs.

7. PdNDs surface coverage, CO-confined growth method.

AFM imaging allows us to conclude that a very remarkable coverage of the **1** surface with metallic nanoparticles has been achieved (Figure S7a). Consequently, a bearing analysis of the recorded AFM images was carried out in order to estimate the percentage of the SAM of **1**-modified surface covered by PdNDs (Figure S7b). AFM images were

reduced to binary images by thresholding with the depth value corresponding to the highest point of the peaks detected in the depth histograms. Thus, the bearing analysis tool allows obtaining the percentage of projected area occupied by features exhibiting depth values smaller than or equal to the thresholded one. The statistical analysis of coverage data registered over 300 x 300 nm^2 areas from 30 different but equivalent AFM images rendered an average PdNDs-coverage of 84.5 ± 2.8 %. A histogram showing surface coverage value distribution is depicted in Figure S7c.

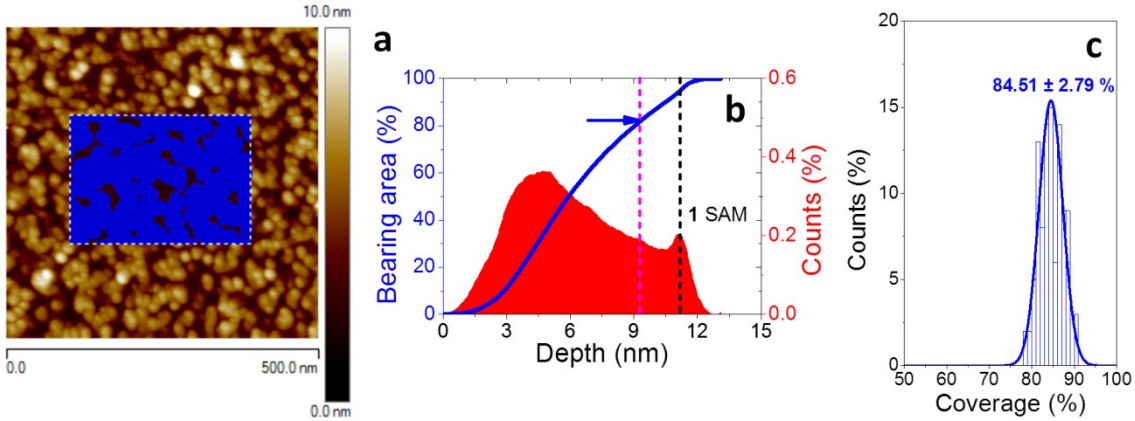

Figure S7. (a) 500 x 500 nm^2 AFM image of gold|SAM (**1**)|PdNDs with the mask in blue unveiling nanodeposit-free **1**-modified areas. (b) Depth histogram showing the distribution of height data at different depth referred to a reference point, i.e. the highest pixel, red line. The blue line (bearing analysis) indicates the relative projected area covered at each depth value depicted as a blue mask in the topographic image corresponding to the white-dashed boxed area. The deepest peak in the red histogram, marked with a black-dashed vertical line, is attributed to the nanodeposit-free **1**-modified substrate while the magenta line accounts for the selected depth threshold corresponding to the lowest maximum peak associated with the height of the measured PdNDs. (c) Histogram showing the average percentage of PdNDs-covered substrate area obtained for fifty equivalent but different 300 x 300 nm^2 AFM images.

8. Surface coverage determined by SEM.

Figure S8 shows the surface coverage as determined from SEM images. The SEM spectra were recorded by using a Quanta FEG-250 SEM microscope from FEI.

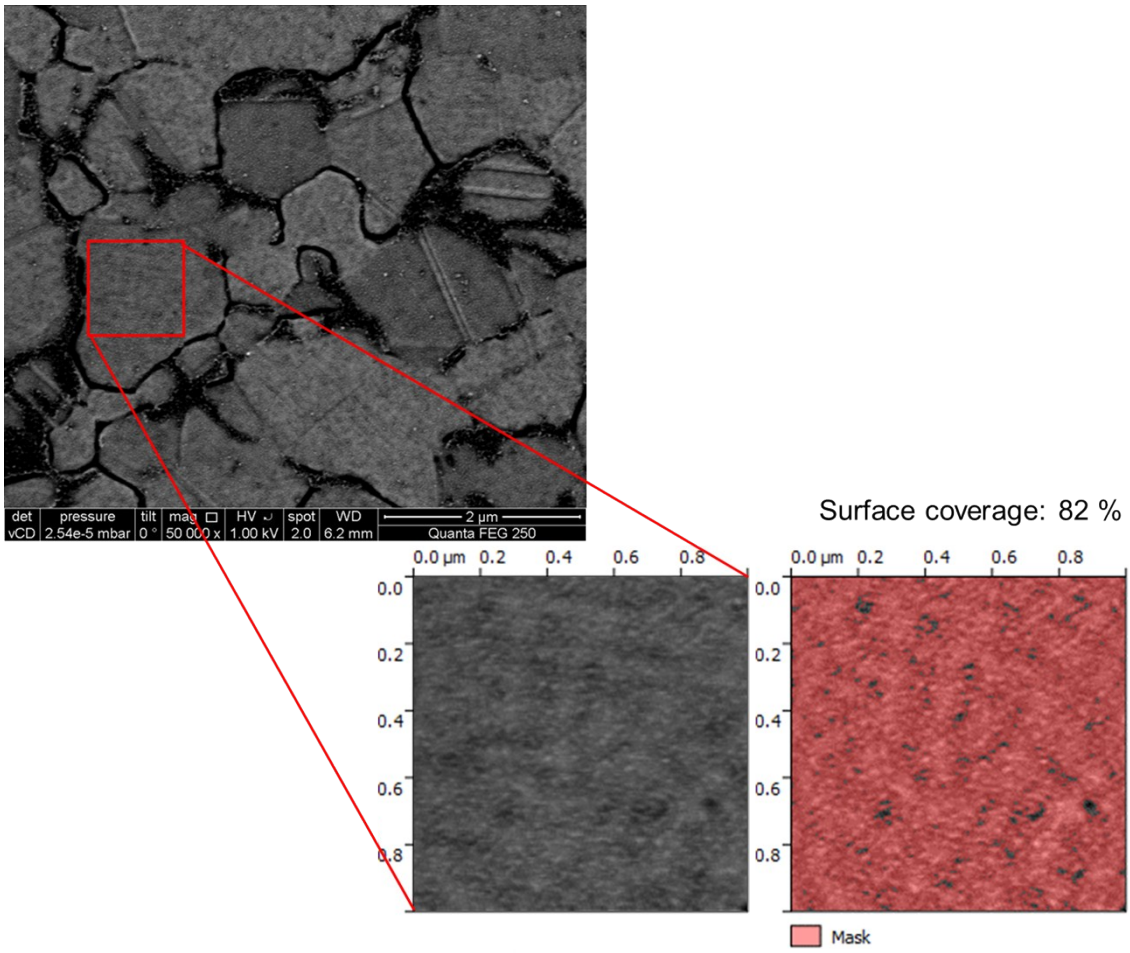

Figure S8. Top: SEM images recorded from a gold|SAM(**1**)|PdNDs system. Bottom left: magnification of the indicated terrace in the pristine SEM image. Bottom right: SEM image with a mask in pink unveiling nanodeposit-free **1**-modified areas.

9. Pd nanosheets surface coverage, immersion in Pd nanosheets method.

After overnight incubation of a gold|SAM (**1**) system in a Pd nanosheet-containing solution (EtOH), AFM images show a remarkably palladium low surface coverage (Figure S9a), in comparison to that obtained when the PdNDs are grown onto the gold|SAM (**1**) in the reaction chamber following the CO-confined growth method, (Figure S6a). Similarly, a bearing analysis of the recorded AFM images was carried out

in order to quantify the percentage of the **1**-modified surface covered by Pd nanosheets (Figure S9b), i.e. 4.96 ± 0.24 %.

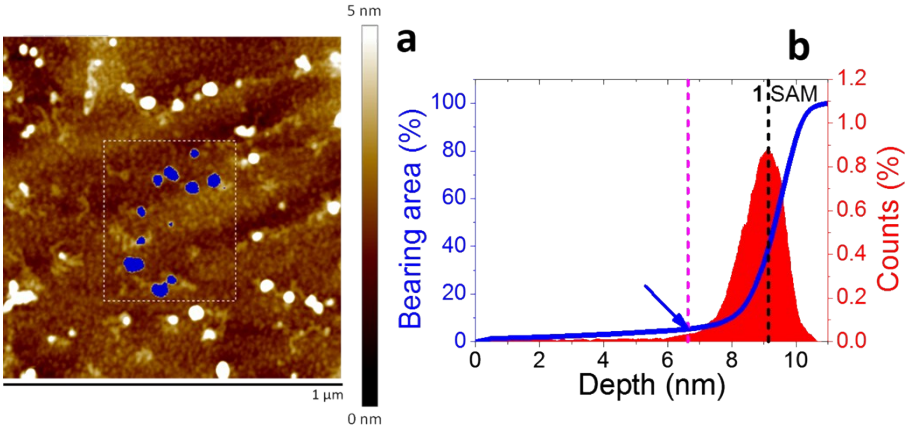

Figure S9. (a) 1.0 x 1.0 µm^2 AFM image of gold|SAM (**1**)|Pd nanosheets with the mask in blue unveiling nanodeposit-free **1**-modified areas. (b) Depth histogram showing the distribution of height data at different depth referred to a reference point, i.e. the highest pixel, red line. The blue line (bearing analysis) indicates the relative projected area covered at each depth value depicted as a blue mask in the topographic image corresponding to the white-dashed boxed area. The deepest peak in the red histogram, marked with a black-dashed vertical line, is attributed to the nanodeposit-free **1**-modified substrate while the magenta line accounts for the selected depth threshold corresponding to the lowest maximum peak associated with the height of the measured PdNDs.

10. *I-V* curves at different set-point forces.

Figure S10 shows *I-V* curves obtained by applying the indicated set-point forces. For low set point forces no significant current is detected. The current increases upon the increasing set-point forces. For the *I-V* curves obtained in the 4-27.3 nN force range studied no sign of short-circuit is observed.

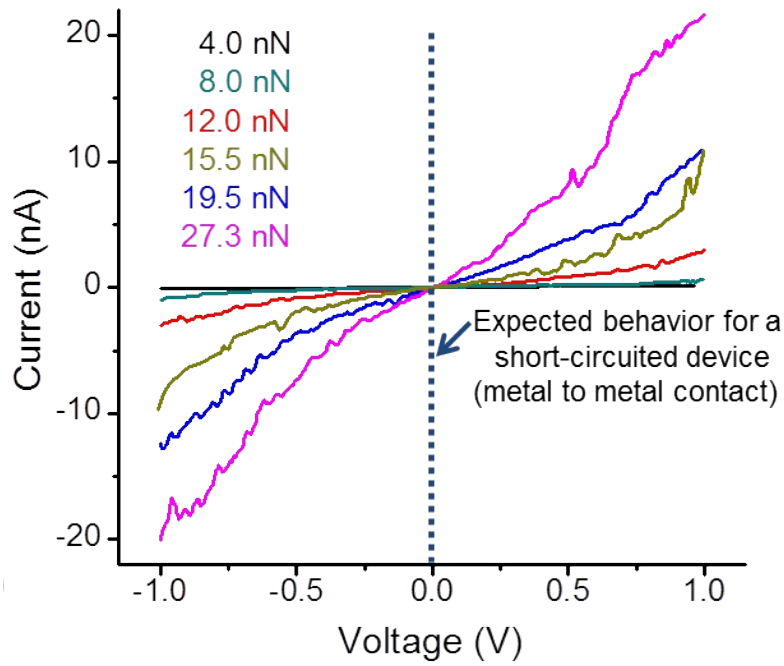

Figure S10. *I-V* curves for the indicated set-point forces.

11. Oxidative desorption of the SAM of 1.

The electrochemical behavior associated with the gold|SAM(**1**)|PdNDs system has been assessed by means of cyclic voltammetry measurements in 0.1 M H_2SO_4. Figure S11 shows the first cycle registered in the anodic direction for the gold|SAM(**1**)|PdNDs system, along with the fifth cycle stabilized voltammogram for the same system. The large, broad and irreversible anodic peak present at very large overpotentials in the first cycle is attributed to the oxidative desorption of OPE moieties adsorbed onto Au(111) substrates.[1-3] Interestingly, after removing electrochemically the SAM of **1** by oxidative desorption, only the characteristic features of the underlying Au(111) substrate electrochemical response can be detected, namely the formation and reduction of the gold monoxide, AuO, monolayer.[4] Therefore, no traces of voltammetric peaks associated with the electrochemical activity of palladium were observed after the

electrochemical removal of the SAM of **1**. In this regard, it should be noted that if hypothetically PdNDs were decorating the bare gold surface, the electroactive area of PdNDs would be much larger than the smooth Au(111) substrate and, consequently, the contributions from the formation of oxide on the underlying Au(111) surface would be almost negligible in comparison to the oxidation of the PdNDs.

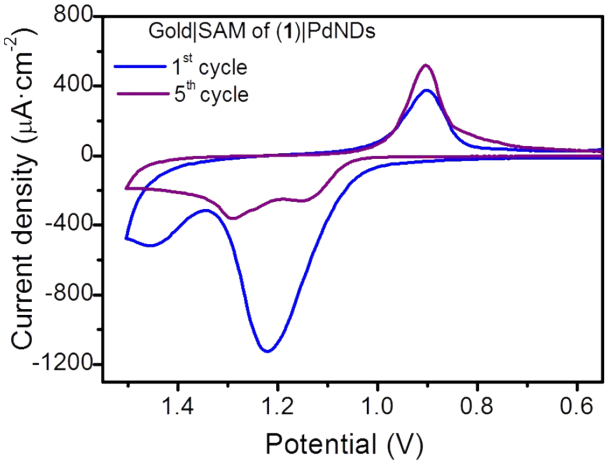

Figure S11. Cyclic voltammograms registered at 0.1 $V \cdot s^{-1}$ in 0.1 M H_2SO_4 for a gold|SAM(**1**)|PdNDs system for the indicated number of cycles. The reference electrode was in both figures Ag/AgCl, KCl (3M).

References

1. Aguilar-Sanchez, R.; Su, G. J.; Homberger, M.; Simon, U.; Wandlowski, T. Structure and electrochemical characterization of 4-Methyl-4′-(n-mercaptoalkyl)biphenyls on Au(111)-(1 × 1). *J. Phys. Chem. C* **2007**, *111*, 17409-17419.
2. Manrique, D. Z.; Huang, C.; Baghernejad, M.; Zhao, X.; Al-Owaedi, O. A.; Sadeghi, H.; Kaliginedi, V.; Hong, W.; Gulcur, M.; Wandlowski, T., et al. A quantum circuit rule for interference effects in single-molecule electrical junctions. *Nat. Communications* **2015**, *6*.
3. Mertens, S. F. L.; Bütikofer, A.; Siffert, L.; Wandlowski, T. Covalent versus electrostatic strategies for nanoparticle immobilisation. *Electroanalysis* **2010**, *22*, 2940-2946.
4. Vericat, C.; Benitez, G. A.; Vela, M. E.; Salvarezza, R. C.; Tognalli, N. G.; Fainstein, A. Restricted surface mobility of thiolate-covered metal surfaces: a simple strategy to produce high-area functionalized surfaces. *Langmuir* **2007**, *23*, 1152-1159.